DOI: 10.1002/cphc.201100686

Three-Dimensional Super-Resolution Imaging of the Midplane Protein FtsZ in Live *Caulobacter crescentus* Cells Using Astigmatism

Julie S. Biteen,[a, b] Erin D. Goley,[c, d] Lucy Shapiro,[c] and W. E. Moerner*[a]

Single-molecule super-resolution imaging provides a non-invasive method for nanometer-scale imaging and is ideally suited to investigations of quasi-static structures within live cells. Here, we extend the ability to image subcellular features within bacteria cells to three dimensions based on the introduction of a cylindrical lens in the imaging pathway. We investigate the midplane protein FtsZ in *Caulobacter crescentus* with super-resolution imaging based on fluorescent-protein photoswitching and the natural polymerization/depolymerization dynamics of FtsZ associated with the Z-ring. We quantify these dynamics and determine the FtsZ depolymerization time to be <100 ms. We image the Z-ring in live and fixed *C. crescentus* cells at different stages of the cell cycle and find that the FtsZ superstructure is dynamic with the cell cycle, forming an open shape during the stalked stage and a dense focus during the pre-divisional stage.

1. Introduction

FtsZ is a tubulin ortholog that is highly conserved in bacterial species. This GTPase is an essential protein that polymerizes at the mid-cell, recruits the division machinery, and may generate constrictive forces necessary for cytokinesis.[1] FtsZ polymerizes into a midplane ring structure (the Z-ring) early in the cell cycle before recruiting the rest of the divisome. In *Caulobacter crescentus*, FtsZ also recruits proteins that direct cell elongation and cellular polarity.[2] Given its importance in cell division, the Z-ring structure is the subject of active investigation, but its subcellular and subwavelength dimensions prevent visualization with conventional fluorescence measurements.[3] Short FtsZ protofilaments were observed at constriction sites in *C. crescentus* by cryo-electron tomography (ET),[4] indicating that the Z-ring structure is not simply a smooth, closed-ring-like structure, but a collection of overlapping protofilaments. Super-resolution (SR) optical imaging techniques are therefore ideally suited for the investigation of the "superstructure", or assembly, formed from the FtsZ filaments.

In single-molecule fluorescence (SMF) imaging, the emission from spatially isolated fluorophores yields high-accuracy information about the position of that fluorophore because the image of a 3–5 nm fluorescent protein (FP) is a reasonable approximation to the point-spread function (PSF) of the microscope.[5] While rigorously a single molecule is an emitting dipole, in practice FP fusions are orientationally mobile, so that the diffraction-limited single-molecule spot in a wide-field fluorescence image can be numerically fit to estimate the *xy* position of the emitter. This technique permits sub-diffraction-limited information to be obtained from diffraction-limited images when single molecules are spaced apart by more than the optical diffraction limit. Applied to live bacterial cells, wide-field SMF microscopy has enabled high-resolution investigations of biomolecule dynamics. For instance, bursts of fluorescence have identified low-level gene expression,[6] and single-molecule tracking experiments have measured the diffusion coefficient of free, cytoplasmic protein and the velocity of motion of polymerized protein.[7] Additionally, freely diffusing cytoplasmic proteins can be captured using very fast acquisition times, however when employing longer acquisition times these fast-moving molecules are not resolved, biasing the camera toward molecules which form quasi-static structures which are stable on the time scale of the imaging.[7] Herein, live-cell SMF imaging is used to characterize the polymerization/depolymerization dynamics of the protein FtsZ, in three spatial dimensions.

With densely packed fluorescent labels, super-resolution (SR) images can be reconstructed from movies where sparse subsets of the molecules are sequentially localized in each movie frame. Importantly, the active emitter density in any frame can be controlled at a low level by photoswitching, photoactivation, cellular dynamics, chemical control, transient dark states, etc.[8–13] Single-molecule SR imaging based on photoactivated

[a] *Dr. J. S. Biteen, Prof. W. E. Moerner*
Department of Chemistry
Stanford University
Stanford, CA 94305 (USA)
E-mail: wmoerner@stanford.edu

[b] *Dr. J. S. Biteen*
Department of Chemistry
University of Michigan
Ann Arbor, MI 48104 (USA)

[c] *Dr. E. D. Goley, Prof. L. Shapiro*
Department of Developmental Biology
Stanford University
Stanford, CA 94305 (USA)

[d] *Dr. E. D. Goley*
Department of Biological Chemistry
Johns Hopkins University
Baltimore, MD 21205 (USA)

Supporting information for this article is available on the WWW under http://dx.doi.org/10.1002/cphc.201100686.

localization microscopy (PALM) has recently been applied to investigations of the FtsZ superstructure in *Escherichia coli*, demonstrating that the Z-ring of *E. coli* is a loose bundle of protofilaments.[14] An alternative SR fluorescence imaging technique, stimulated emission depletion (STED) microscopy, has yielded consistent results for FtsZ rings in fixed *Bacillus subtilis* cells stained with an anti-FtsZ antibody.[15]

A variety of SR techniques have been applied to biomolecular structures in cells. Wide-field cellular imaging is generally limited to the thin surface layer next to the coverslip by the need to use a total-internal reflection (TIRF) microscope geometry, though thicker cells have been examined with Bessel beams and two-photon selective excitation.[16] Due to their thin (~micron-diameter) size, the entirety of bacterial cells can be imaged in wide-field without TIRF.[7] Still, most experiments have been limited to a two-dimensional projection of the three-dimensional sample. Methods to extend wide-field, single-molecule-based SR imaging to three dimensions include astigmatism,[17,18] multiplane methods,[19] optical sectioning,[20] interferometry,[21] and double-helix point-spread function microscopy.[22]

Here, we use optical astigmatism to gain axial (z) information for each single-molecule fit.[17,18] The astigmatism is introduced via a weak cylindrical lens in the emission pathway of the wide-field single-molecule microscope. In the presence of this lens, the detected PSF from a single-molecule is asymmetric, and in addition to localizing the molecule in the xy plane based on the center of the PSF, the degree of PSF asymmetry indicates the axial position of the molecule. For fluorescent protein fusions in *C. crescentus* cells, the ability of the astigmatic single-molecule microscope to resolve axial molecular positions with <100 nm z localization precision promises to shed light on macromolecular structure in three dimensions.

2. Results and Discussion

2.1. Characterization of the FtsZ polymerization/depolymerization dynamics in live and fixed *Caulobacter crescentus*

Cultures of a *C. crescentus* merodiploid strain containing the wild-type (WT) *ftsZ* gene and a single chromosomal copy of a *ftsZ-dendra2* fusion under the control of a xylose-inducible promoter were incubated in a xylose concentration selected to give rise to expression of $\sim 10^2$–10^3 Dendra2-labeled FtsZ fusion proteins per cell. These cells were mounted directly on an agarose pad for live-cell imaging, or fixed in formaldehyde (Supporting Information) for immobilization before sample preparation. The fixed and live cells were imaged with 561 nm laser excitation, at which wavelength the green form of the green-to-red photoswitchable fluorescent protein Dendra2 is not observed.[23] Initially, the cells were therefore non-fluorescent, but following a dose of 407 nm laser illumination (0.5 s at 2000 W cm^{-2}, chosen to photoswitch only a small subset of the Dendra2 molecules such that at most one molecule was observed per diffraction-limited spot), isolated single FtsZ-Dendra2 molecules were observed and localized with <30 nm precision, and their positions were recorded. After imaging, localizing, and photobleaching all photoswitched molecules, the 407 nm pulse was reapplied such that a new subset of FtsZ-Dendra2 molecules became visible. Cycles of photoswitching, imaging, and bleaching were repeated for 15 s.

Due to the small size of the FtsZ superstructure, only 1–2 FtsZ molecules can be simultaneously localized in the Z-ring given the need for isolated PSFs in any single frame. However, knowledge of the polymerization/depolymerization dynamics of the FtsZ molecules was used to increase the number of localization events possible after each photoswitching pulse by several orders of magnitude. In live-cell experiments, freely diffusing cytoplasmic proteins cannot be resolved with EMCCD acquisition times greater than 5–10 ms as their emission signal is spread out over many camera pixels. Here, 15 ms integration times captured only those FtsZ molecules having motion slowed by polymerization. Photoactivated freely diffusing cytoplasmic FtsZ-Dendra2 molecules appear invisible, but when the same molecule is incorporated into a protofilament, it becomes visible. Conversely, polymerized, visible FtsZ-Dendra2 molecules become invisible upon depolymerization.

Bulk-level studies have shown FtsZ to be very dynamic in vivo, turning over rapidly.[24,25] In our studies, a fresh supply of FtsZ-Dendra2 molecules was therefore incorporated into the Z-ring regularly, and many molecular positions could be obtained before an additional photoswitching pulse was required. In this way, more than 10^4 single molecules were localized with 30 nm or better statistical localization precision over the course of 1000 imaging frames (15 s).

The dynamics of the FtsZ polymerization/depolymerization were examined for a representative live stalked cell and contrasted with findings for a representative fixed stalked cell. Figure 1 A gives the distribution of Dendra2 visibility times for

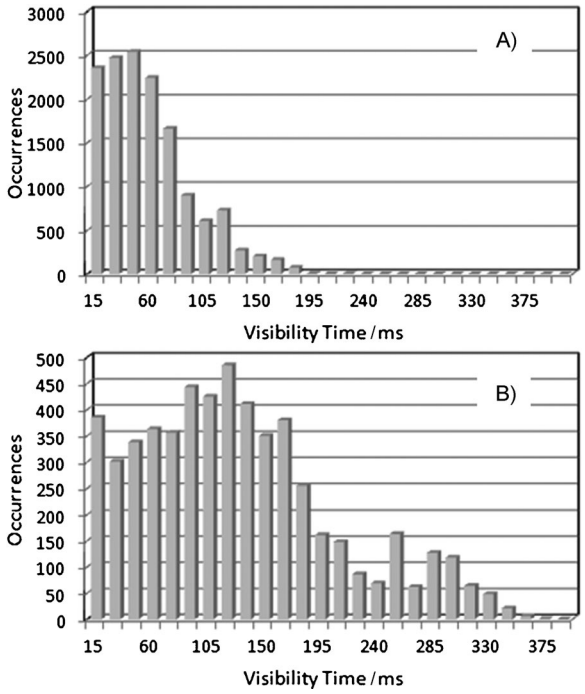

Figure 1. Visibility times for FtsZ-Dendra2 in A) live *C. crescentus* cells and B) fixed *C. crescentus* cells.

14212 imaged molecules in a live stalked cell. Here, the visibility time is determined by extracting the number of continuous frames over which a molecule is localized in the same diffraction-limited spot. The average visibility time for FtsZ-Dendra2 in live cells is 58 ms. The mechanism for becoming visible is photoswitching or polymerization and the mechanism for becoming invisible can be photobleaching or depolymerization.

Figure 1 B gives the distribution of Dendra2 visibility times for 5566 molecules imaged in a fixed stalked cell. Here, the sole mechanism for becoming visible is photoswitching and the only mechanism for becoming invisible is photobleaching, and so the visibility time is in this case the photobleaching time of the molecule. The average visibility time in fixed cells is 128 ms. The shorter visibility times for molecules in live cells are attributed to fast depolymerization. By comparing the 58 ms average visibility time of FtsZ-Dendra2 in live cells to the 128 ms average photobleaching time of FtsZ-Dendra2 in fixed cells (where depolymerization could not occur), the depolymerization time of FtsZ in the *C. crescentus* Z-ring was determined to be $< \sim 100$ ms. This is much shorter than the ~8–9 s half-life of FtsZ molecules in the Z-ring in *E. coli* and *B. subtilis* determined by fluorescence recovery after photobleaching (FRAP),[24] indicating that in addition to new FtsZ molecules coming to the midplane every few seconds, these midplane-localized FtsZ are highly dynamic on a faster timescale, polymerizing and depolymerizing in under 100 ms.

2.2. Two-Dimensional Super-Resolution Imaging of FtsZ in Live *Caulobacter crescentus*

Live *C. crescentus* cells expressing FtsZ-Dendra2 were prepared as in Section 2.1. For initial two-dimensional (2D) imaging, the positions of all localized FtsZ molecules with localization precision better than 30 nm (as given by the statistical 95% confidence interval of the center of the PSF based on a fit to a 2D Gaussian function, as described previously)[26] were used to form the reconstructed image of the FtsZ superstructures in Figure 2. Here, each molecule is plotted as a Gaussian profile with fixed standard deviation, $\sigma = 30$ nm, and with amplitude proportional to the inverse of the localization precision of that molecule, that is, molecules which localized better are shown brighter in the reconstruction. The cell population in Figure 2 is not synchronized and several stages of the cell cycle are therefore accessed simultaneously over a wide field-of-view, a property that is difficult to achieve with ET, for example. From bulk-level diffraction-limited fluorescence microscopy, FtsZ is seen to localize rapidly to the Z-ring at the cell mid-plane at the start of the cell cycle and persist.[3] With its improved resolution, Figure 2 distinguishes between the superstructure of FtsZ in stalked cells (e.g. red box) and in pre-divisional cells (e.g. blue box).

64 cells that each had 300 or more single-molecule localizations were analyzed, and we distinguished between FtsZ structures with transverse width wider than 500 nm (stalked cells, $N = 41$) and structures narrower than 500 nm (pre-divisional cells, $N = 23$). FtsZ in the stalked cells appears as a thin line at the mid-plane in the 2D images. These stalked cell structures

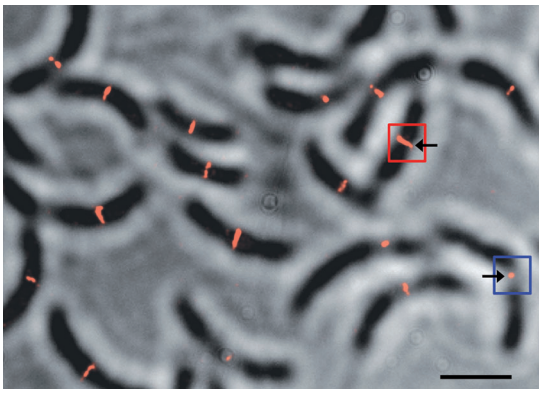

Figure 2. False-color two-dimensional SR reconstruction of FtsZ-Dendra2 (red) in live *C. crescentus* cells overlaid on a reversed contrast white-light transmission image of the cells. The red box highlights the midplane of a stalked cell; here, the arrow points to the FtsZ ring typically observed in stalked cells. The blue box highlights the midplane of a pre-divisional cell; here, the arrow points to the FtsZ constriction typically observed in pre-divisional cells. Scale bar: 2 μm.

ranged in longitudinal thickness from 63–107 nm and had an average thickness of 67 nm. The representative stalked cell structure in the red box in Figure 2 has a thickness of 69 nm (cross section in Figure S6C, Supporting Information). The measured thicknesses are convoluted with the measurement resolution, but the stalked cell structures are consistently thicker than the 30 nm experimental resolution. Since the protofilaments are 5 nm in width,[4] this observation of a thick ring is attributed to the presence of many filaments. Unfortunately, since the size of *C. crescentus* is significantly smaller than that of *E. coli*, the structure of the filaments is not resolved, but the large thickness is consistent with the model of loose bundles of short, overlapping FtsZ protofilaments at the Z-ring proposed by Fu et al. and Erickson et al.[1,14] The cytoskeletal FtsZ Z-ring is anchored to the inner membrane and aids cell invagination.

In the 23 pre-divisional cells, the FtsZ superstructure looks like a constricted mass and not a thin line. The average thickness of these pre-divisional cell FtsZ structures along the longitudinal axis was 92 nm, with measured widths ranging from 72–133 nm. These pre-divisional cell structures are significantly thicker than those observed in stalked cells. As the cell is constricted, the Z-ring thickens on the long axis of the cell, perhaps because the increased cell length at this length stage leads to increased distance from the polar negative regulator, MipZ or perhaps due to changes in inner membrane geometry during constriction. The representative deeply constricted pre-divisional cell structure in the blue box in Figure 2 has a thickness of 86 nm (cross section in Figure S6D, Supporting Information). The tightly focused FtsZ structure is roughly symmetric along the transverse and longitudinal cell axes.

2.3. Three-Dimensional Super-Resolution Imaging of FtsZ in Live *Caulobacter crescentus*

To gain further insight into the FtsZ superstructures appearing as thin lines (stalked cells) and constricted foci (pre-divisional

cells) in two-dimensional SR imaging (Figure 2), a 1 m focal distance cylindrical lens was introduced into the imaging pathway of the wide-field microscope in order to add astigmatism to the single-molecule PSFs.[17,27] The imaging system was calibrated with fluorescent beads on a coverslip. Using a piezoelectric microscope objective scanner (PIFOC), the fluorescent bead PSFs were recorded as a function of defocus and the degree of astigmatism was fit to an analytical defocusing function. With a correction for difference in the index of refraction between the calibration substrate and the *C. crescentus* sample,[28] this defocusing curve could then be used to localize single-molecules in the axial (*z*) position as well as in-plane (see the Supporting Information).

Samples of live *C. crescentus* cells were prepared in a manner identical to Section 2.1, and imaged in the astigmatic SR imaging microscope under the same conditions as in Section 2.1. Here, the emitter PSFs were each fit with an asymmetric 2D Gaussian function. The center of each Gaussian corresponds to the in-plane (*x,y*) position and the aspect ratio of the *x* width of each Gaussian to its *y* width indicates the axial (*z*) position. Again, the error in (*x,y*) is given by the statistical 95% confidence interval on the center position, and only molecules with <30 nm localization precision are considered. The error in the *z* position is found based on the standard deviation of subsequent localizations of the same molecule (Supporting Information). Consistent with Badieirostami et al.,[29] the localization precision of the molecules is dependent on *z* and is best at the focus (Figure S1, Supporting Information). The precision of the *z* position is <100 nm for all the molecules considered; far below the axial diffraction limit of 572 nm. Since the localization precision in *z*, like the precision in (*x,y*), is dependent on the number of photons per frame collected from each molecule[30] (here 50–200 photons), this axial localization precision would be improved for brighter signals; indeed at the focal plane, a 15–20 nm precision is expected for 1000 collected photons.[29]

The FtsZ superstructure in the live stalked cell studied in Figure 1A is shown in Figure 3. The positions of 14212 3D localizations of FtsZ proteins collected over 15 s in a single live stalked cell were used to form the reconstructed image. A video showing this 3D image over 360 degrees is provided in the Supporting Information. Figure 3 shows projections of this image along the *xy* plane (Figure 3A) and the *xz* plane (Figure 3B). Here, each localization is represented as a 2D Gaussian with intensity proportional to total number of photons collected and with a uniform width of 20 nm. The y-axis corresponds to the long axis of the cell being investigated. The *xy* view in Figure 3A corresponds well with the typical 2D SR image of FtsZ superstructure in stalked cells (red box in Figure 2), while the *xz* view in Figure 3B shows the cross-sectional view that is lost in 2D imaging. This cross-sectional view clearly shows that the Z-ring in this stalked cell spans the cell diameter (~650 nm) and has a ~150 nm opening at the center. The thickness of the torus is consistent with the presence of a loose 3D bundle extending away from the membrane into the cytoplasm.[14]

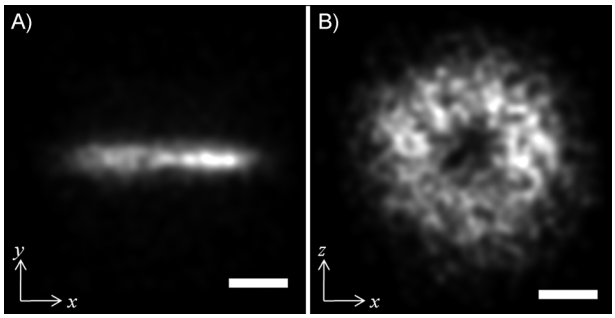

Figure 3. 2D Projections of 3D SR images of FtsZ-Dendra2 in a live stalked cell oriented lengthwise along the y axis in A) the *xy*-plane (i.e. top view; typical of 2D SR images) and B) the *xz*-plane (i.e. cross-sectional view). Scale bar: 200 nm.

The positions of all 3D localized FtsZ proteins in a representative live pre-divisional cell are used to form a second reconstructed image. A video showing this image from 360 degrees is provided in the Supporting Information. Figure 4 shows the projections of this image along the *xy* plane (A) and the *xz* plane (B). Here, each localization is represented as a 2D Gaussian with intensity proportional to total number of photons collected and with a uniform width of 20 nm and the y-axis corresponds to the long axis of the cell being investigated. The *xy* view in Figure 4A corresponds well with the typical 2D SR image of FtsZ superstructure in pre-divisional cells (blue box in Figure 2), while the *xz* view in Figure 4B shows the cross-sectional view that is unavailable in 2D imaging. This cross sectional view clearly shows that the constricted Z-ring focus in this pre-divisional cell is roughly symmetric in all directions with a diameter of ~150 nm, consistent with the Z-ring thickening along the longitudinal cell axis as it constricts.

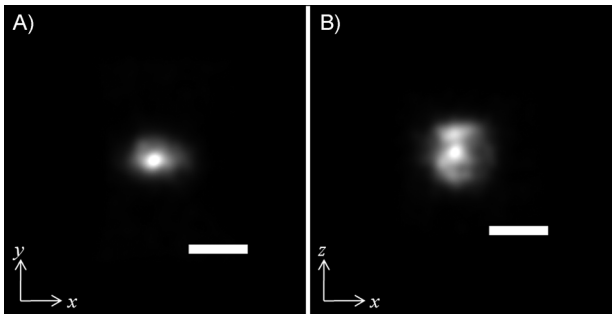

Figure 4. 2D Projections of 3D SR images of FtsZ-Dendra2 in a live pre-divisional cell oriented lengthwise along the *y*-axis in A) the *xy*-plane i.e. top view; typical of 2D SR images) and B) the *xz*-plane (i.e. cross-sectional view). Scale bar: 200 nm.

2.4. Three-Dimensional Super-Resolution Imaging of FtsZ in Fixed *Caulobacter crescentus*

C. crescentus cells expressing FtsZ-Dendra2 were prepared as in Section 2.1, then fixed with formaldehyde (Supporting Information) for immobilization before imaging. Whereas in the live-

cell samples, only slowly moving (polymerized) FtsZ molecules are localized, all fluorescently labeled FtsZ molecules are immobilized, and therefore potentially capable of being imaged, in fixed cells. Consequently, only a few FtsZ-Dendra2 molecules could be photoswitched to the emissive state with each 407 nm laser pulse since otherwise too many active molecules would be imaged at once. The fixed cells were therefore imaged in the 3D microscope as described in Section 2.3, but with a 20-fold weaker 407 nm photoswitching laser dose (500 $W cm^{-2}$ for 0.1 s rather than 2000 $W cm^{-2}$ for 0.5 s). As in section 2.3, all single-molecule positions were recorded and the SR image reconstructed. A video is provided in the Supporting Information showing the reconstruction over 360 degrees of viewing angle.

The FtsZ localizations in the fixed, stalked cell studied in Figure 1 B are compiled into a SR image in Figure 5, which shows an open Z-ring with ~250 nm opening much like the live, stalked cell image in Figure 3. However, the large number of freely diffusing cytoplasmic FtsZ molecules localized in the fixed cell give rise to an effective background that is not seen in live cells. In addition to having more localizations due to cytoplasmic proteins, the localization precision of cytoplasmic FtsZ and Z-Ring FtsZ in the fixed stalked cell is roughly equal (Figure S4, Supporting Information) while the localization precision of the few cytoplasmic FtsZ molecules localized in the live stalked cell is much lower (Figure S2, Supporting Information). Figures S2 and S4 depict the same structures as Figures 3 and 5, but use dots instead of Gaussian functions to represent each of the 5566 localization events.

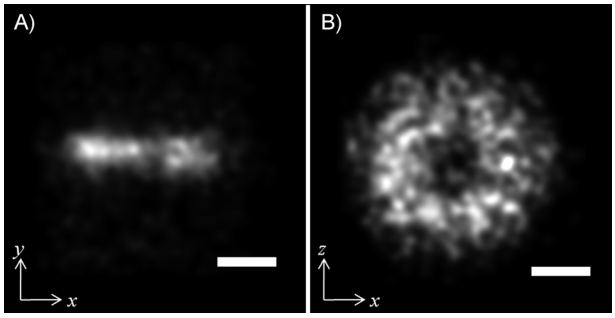

Figure 5. 2D Projections of 3D SR images of FtsZ-Dendra2 in a fixed stalked cell oriented lengthwise along the *y*-axis in A) the *xy*-plane (i.e. top view; typical of 2D SR images) and B) the *xz*-plane (i.e. cross-sectional view). Scale bar: 200 nm.

Similarly, the representative fixed, pre-divisional cell SR reconstruction image in Figure 6 shows a constricted focus that is symmetric in all directions with a diameter of ~200 nm analogous to that in the live pre-divisional cell of Figure 4, but again, due to the lack of contrast between cytoplasmic and polymerized FtsZ, more localizations outside of the superstructure are evident. This is also observed in Figures S3 and S5 (Supporting Information), which depict the same structures as Figure 4 and 6, but with dots instead of Gaussians for each localization event.

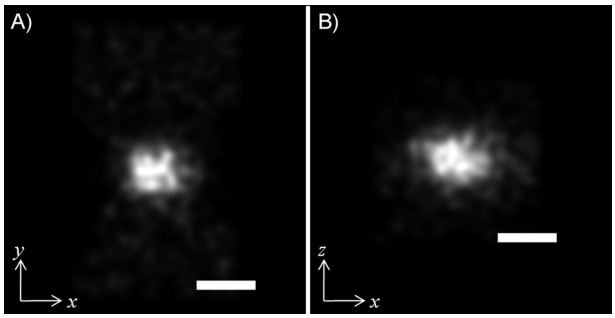

Figure 6. 2D Projections of 3D SR images of FtsZ-Dendra2 in a fixed pre-divisional cell oriented lengthwise along the y axis in A) the *xy*-plane (i.e. top view; typical of 2D SR images) and B) the *xz*-plane (i.e. cross-sectional view). Scale bar: 200 nm.

3. Conclusions

We describe the first application of 3D astigmatic super-resolution imaging to a dynamical system where single-molecule imaging is used to discern the natural dynamics of the proteins under investigation. By using wide-field SMF imaging to detect only polymerized FtsZ molecules, the depolymerization time of FtsZ in the Z-ring was determined to be under 100 ms, significantly faster than the 8–9 s half-life measured by FRAP in *E. coli and B. subtilis*.[24] In addition to new FtsZ molecules coming to the midplane every few seconds, these midplane-localized FtsZ are highly dynamic on the sub-second timescale.

This natural dynamical motion, which provides new polymerized (and therefore detectable) FtsZ-Dendra2 molecules every ~100 ms, complements photoswitching in super-resolution imaging. By performing super-resolution imaging based on using both photoswitching of Dendra2 and the FtsZ polymerization/depolymerization dynamics, the superstructure of the FtsZ Z-ring in *C. crescentus* cells was resolved with <30 nm lateral resolution and <100 nm axial resolution based on single-molecule SR imaging and astigmatism. In addition to enabling studies of the unperturbed system and taking advantage of the dynamics to increase the number of molecules localized, an additional benefit of studying live *C. crescentus* cells is that the Dendra2 fluorescent proteins in this system are not highly constrained due to the floppy tether to FtsZ, thereby avoiding decreases in localization accuracy due to constrained molecular orientation.[31]

Typical Z-rings in stalked cells were found to span the diameter of the cell, to have widths of 70–100 nm and to show ring openings of 150–300 nm, consistent with a compressed helix or other structure comprised of a large number protofilaments. The cell-cycle dependent structure was investigated, and Z-rings in pre-divisional cells were found to be constricted into tight, symmetric foci with diameters as small as 150 nm, and with no obvious opening at the center. The 15 s imaging time demonstrated here is sufficient for assessing the 3D shape of the FtsZ assembly at multiple time points within the 150 min cell cycle.

Because bacterial cells are naturally as thin as the depth of focus of a high-NA microscope (~1 μm), the straightforward introduction of a cylindrical lens into the microscopy emission

pathway is a useful way to image protein superstructure in prokaryotic cells in 3D. Combining this 3D astigmatic microscope with live-cell imaging, where knowledge of the natural dynamics of the molecules allows slowly moving macromolecules to be differentiated from more rapidly diffusing molecules, leads to increased numbers of localizations and therefore higher-resolution images.

Experimental Section

Cultures of the *C. crescentus* merodiploid strain containing WT *ftsZ* and a chromosomal copy of *ftsZ-dendra2* were grown at 28 °C in PYE media then in M2G minimal media. After a 1 h incubation in 0.015% xylose, cells were added directly to an agarose pad (1.5% in M2G) (live-cell experiments), or fixed in 1% formaldehyde before being added to the agarose pad (fixed-cell experiments). TetraSpeck fluorescent microspheres (Invitrogen Molecular Probes) added to the agarose pads served as fiduciary markers.

Cells were imaged with a 1.41 NA oil-immersion objective in an Olympus IX71 inverted microscope and detected on a 512× 512 pixel Andor Ixon EMCCD at a rate of 15 ms/frame. Subpopulations of FtsZ-Dendra2 were switched to their red state by a dose of 407 nm light (Coherent Innova 300 Kr^+ laser) chosen to photoswitch only a sparse subset of the Dendra2. The red FtsZ-Dendra2 fusions were imaged with 561 nm light (Crystalaser CL561-025-O) until photobleaching occurred, and the photoswitching/imaging cycle was repeated. The wide-field epifluorescence setup has been described previously,[26,32] and was adapted for 561 nm imaging with appropriate filters (Semrock Di-01-561 and Semrock BLP01-561R). For the 3D astigmatic acquisitions, a 1 m focal length cylindrical lens was placed in the microscope emission pathway 2.0 cm before the usual imaging plane, and the camera position was adjusted for focus.

Positions of isolated FtsZ-Dendra2 fusions were determined from a fit to a 2D Gaussian function. The *xy* position corresponds to the peak position of the fit, and the statistical precision of each *xy* localization is given by the 95% confidence interval from the fit. For the 3D imaging, the *z* position is given by the ratio of the fit standard deviations in the *x* and *y* dimensions, σ_x/σ_z. The relationship between *z* and σ_x/σ_z is calibrated using a sample consisting of a fiduciary markers on a coverslip, fit to an analytical defocusing equation, and corrected for differences in refractive index (see Supporting Information).

Acknowledgements

Thanks to Steven Lee for assistance with 3D figure generation. This work was supported by Award No. R01GM086196 from the National Institute of General Medical Sciences (W.E.M., L.S.) and by a Burroughs Wellcome Career Award at the Scientific Interface (J.S.B.).

Keywords: astigmatic lens · live-cell imaging · proteins · single-molecule studies · three-dimensional imaging

[1] H. P. Erickson, D. E. Anderson, M. Osawa, *Microbiol. Mol. Biol. Rev.* **2010**, *74*, 504 – 528.
[2] E. D. Goley, Y. C. Yeh, S. H. Hong, M. J. Fero, E. Abeliuk, H. H. McAdams, L. Shapiro, *Mol. Microbiol.* **2011**, *80*, 1680 – 1698.
[3] M. Thanbichler, L. Shapiro, *Cell* **2006**, *126*, 147 – 162.
[4] Z. Li, M. J. Trimble, Y. V. Brun, G. J. Jensen, *EMBO J.* **2007**, *26*, 4694 – 4708.
[5] W. E. Moerner, *Nat. Methods* **2006**, *3*, 781 – 782.
[6] J. Yu, J. Xiao, X. Ren, K. Lao, X. S. Xie, *Science* **2006**, *311*, 1600 – 1603.
[7] S. Y. Kim, Z. Gitai, A. Kinkhabwala, L. Shapiro, W. E. Moerner, *Proc. Natl. Acad. Sci. USA* **2006**, *103*, 10929 – 10934.
[8] E. Betzig, G. H. Patterson, R. Sougrat, O. W. Lindwasser, S. Olenych, J. S. Bonifacino, M. W. Davidson, J. Lippincott-Schwartz, H. F. Hess, *Science* **2006**, *313*, 1642 – 1645.
[9] M. J. Rust, M. Bates, X. Zhuang, *Nat. Methods* **2006**, *3*, 793 – 796.
[10] S. T. Hess, T. P. K. Girirajan, M. D. Mason, *Biophys. J.* **2006**, *91*, 4258 – 4272.
[11] A. Sharonov, R. M. Hochstrasser, *Proc. Natl. Acad. Sci. USA* **2006**, *103*, 18911 – 18916.
[12] J. Vogelsang, T. Cordes, C. Forthmann, C. Steinhauer, P. Tinnefeld, *Proc. Natl. Acad. Sci. USA* **2009**, *106*, 8107 – 8112.
[13] S. F. Lee, M. A. Thompson, M. A. Schwartz, L. Shapiro, W. E. Moerner, *Biophys. J.* **2011**, *100*, L31 – L33.
[14] G. Fu, T. Huang, J. Buss, C. Coltharp, Z. Hensel, J. Xiao, *PLoS One* **2010**, *5*, e12680.
[15] P. C. Jennings, G. C. Cox, L. G. Monahan, E. J. Harry, *Micron* **2011**, *42*, 336 – 341.
[16] T. A. Planchon, L. Gao, D. E. Milkie, M. W. Davidson, J. A. Galbraith, C. G. Galbraith, E. Betzig, *Nat. Methods* **2011**, *8*, 417 – 423.
[17] B. Huang, W. Wang, M. Bates, X. Zhuang, *Science* **2008**, *319*, 810 – 813.
[18] S. A. Jones, S. Shim, J. He, X. Zhuang, *Nat. Methods* **2011**, *8*, 499 – 505.
[19] M. F. Juette, T. J. Gould, M. D. Lessard, M. J. Mlodzianoski, B. S. Nagpure, B. T. Bennett, S. T. Hess, J. Bewersdorf, *Nat. Methods* **2008**, *5*, 527 – 529.
[20] J. Fölling, V. Belov, R. Kunetsky, R. Medda, A. Schönle, A. Egner, M. Bossi, S. W. Hell, *Angew. Chem.* **2007**, *119*, 6382 – 6386; *Angew. Chem. Int. Ed.* **2007**, *46*, 6266 – 6270.
[21] G. Shtengel, J. A. Galbraith, C. G. Galbraith, J. Lippincott-Schwartz, J. M. Gillette, S. Manley, R. Sougrat, C. M. Waterman, P. Kanchanawong, M. W. Davidson, R. D. Fetter, H. F. Hess, *Proc. Natl. Acad. Sci. USA* **2009**, *106*, 3125 – 3130.
[22] S. R. P. Pavani, M. A. Thompson, J. S. Biteen, S. J. Lord, N. Liu, R. J. Twieg, R. Piestun, W. E. Moerner, *Proc. Natl. Acad. Sci. USA* **2009**, *106*, 2995 – 2999.
[23] N. G. Gurskaya, V. V. Verkhusha, A. S. Shcheglov, D. B. Staroverov, T. V. Chepurnykh, A. F. Fradkov, S. Lukyanov, K. A. Lukyanov, *Nat. Biotechnol.* **2006**, *24*, 461 – 465.
[24] D. E. Anderson, F. J. Guieros-Filho, H. P. Erickson, *J. Bacteriol.* **2004**, *186*, 5775 – 5781.
[25] J. Stricker, P. Maddox, E. D. Salmon, H. P. Erickson, *Proc. Natl. Acad. Sci. USA* **2002**, *99*, 3171 – 3175.
[26] J. S. Biteen, M. A. Thompson, N. K. Tselentis, G. R. Bowman, L. Shapiro, W. E. Moerner, *Nat. Methods* **2008**, *5*, 947 – 949.
[27] H. P. Kao, A. S. Verkman, *Biophys. J.* **1994**, *67*, 1291 – 1300.
[28] Y. Deng, J. W. Shaevitz, *Appl. Opt.* **2009**, *48*, 1886 – 1890.
[29] M. Badieirostami, M. D. Lew, M. A. Thompson, W. E. Moerner, *Appl. Phys. Lett.* **2010**, *97*, 161103.
[30] R. E. Thompson, D. R. Larson, W. W. Webb, *Biophys. J.* **2002**, *82*, 2775 – 2783.
[31] J. Engelhardt, J. Keller, P. Hoyer, M. Reuss, T. Staudt, S. W. Hell, *Nano Lett.* **2011**, *11*, 209 – 213.
[32] W. E. Moerner, D. P. Fromm, *Rev. Sci. Instrum.* **2003**, *74*, 3597 – 3619.

Received: September 6, 2011
Revised: December 16, 2011
Published online on January 20, 2012

